Micro–adhesion rings surrounding TCR microclusters are essential for T cell activation

Akiko Hashimoto-Tane,[1] Machie Sakuma,[1] Hiroshi Ike,[1,3] Tadashi Yokosuka,[1] Yayoi Kimura,[4] Osamu Ohara,[2,5] and Takashi Saito[1,3]

[1]Laboratory for Cell Signaling and [2]Laboratory for Integrative Genomics, RIKEN Center for Integrative Medical Sciences, Yokohama, Kanagawa 230-0045, Japan
[3]Laboratory for Cell Signaling, World Premier International Immunology Frontier Research Center, Osaka University, Suita, Osaka 565-0871, Japan
[4]Advanced Medical Research Center, Yokohama City University, Yokohama, Kanagawa 236-0004, Japan
[5]Kazusa DNA Research Institute, Kisarazu, Chiba 292-0818, Japan

The immunological synapse (IS) formed at the interface between T cells and antigen-presenting cells represents a hallmark of initiation of acquired immunity. T cell activation is initiated at T cell receptor (TCR) microclusters (MCs), in which TCRs and signaling molecules assemble at the interface before IS formation. We found that each TCR-MC was transiently bordered by a ring structure made of integrin and focal adhesion molecules in the early phase of activation, which is similar in structure to the IS in microscale. The micro–adhesion ring is composed of LFA-1, focal adhesion molecules paxillin and Pyk2, and myosin II (MyoII) and is supported by F-actin core and MyoII activity through LFA-1 outside-in signals. The formation of the micro–adhesion ring was transient but especially sustained upon weak TCR stimulation to recruit linker for activation of T cells (LAT) and SLP76. Perturbation of the micro–adhesion ring induced impairment of TCR-MC development and resulted in impaired cellular signaling and cell functions. Thus, the synapse-like structure composed of the core TCR-MC and surrounding micro–adhesion ring is a critical structure for initial T cell activation through integrin outside-in signals.

When T cells recognize an antigen (Ag) MHC on APCs by their TCRs, TCR microclusters (MCs) are generated at the interface and recruit kinases and adapters to initiate activation signals. The TCR-MCs move to the center of the interface to form the central supramolecular activation cluster (SMAC [cSMAC]), generating the bull's eye–type immunological synapse (IS; Bunnell et al., 2002; Campi et al., 2005; Yokosuka et al., 2005; Saito and Yokosuka, 2006; Hashimoto-Tane et al., 2011). Because most membrane-proximal signaling molecules critical for T cell activation, such as ZAP70 (ζ-chain–associated kinase protein 70 kD), LAT (linker for activation of T cells), SLP76 (SH2 domain–containing leukocyte protein of 76 kD), PLC-γ (phospholipase Cγ), etc., are recruited to TCR-MCs, the quality and quantity of the activation depends on regulation of these structures (Yokosuka et al., 2005; Čemerski et al., 2007). However, how the signaling complexes translate signal strength to lead to different outcomes is still largely unknown.

T cell activation primarily requires integrin-mediated conjugate formation between T cells and APCs. Activation of LFA-1, the major integrin expressed on T cells (Dustin et al., 1997), is triggered by the inside-out signal from TCR or chemokine stimulation. A further change into the high-affinity conformation of LFA-1 is mediated by the outside-in signal upon binding to its ligand intercellular adhesion molecule 1 (ICAM-1; Springer and Dustin, 2012). LFA-1–deficient (KO) mice have reduced sensitivity to Ag (Perez et al., 2003; Wang et al., 2008), although the in vivo responses of the KO mice differ depending on the experimental systems (Schmits et al., 1996; Eskan et al., 2012). In the context of the IS, LFA-1 and its ligand ICAM-1 accumulate outside of the cSMAC as the peripheral SMAC (Monks et al., 1998; Grakoui et al., 1999; Krummel et al., 2000). Recently, it was revealed that all three LFA-1 activation states, low-, medium-, and high-affinity forms, are present at the peripheral SMAC (Comrie et al., 2015). The integrin-mediated outside-in signal induces activation of kinases and clustering of SLP76 (Perez et al., 2003; Baker et al., 2009). However, how the LFA-1–mediated outside-in signal contributes to T cell activation remains unclear.

In general, integrin signals activate focal adhesion molecules (Mitra et al., 2005). The major components, talin, paxillin (Pxn), and tyrosine kinase Pyk2, have been observed at the IS (Monks et al., 1998; Sancho et al., 2002; Robertson

Correspondence to Takashi Saito: takashi.saito@riken.jp; or Akiko Hashimoto-Tane: akiko.tane@riken.jp

T. Yokosuka's present address is Dept. of Immunology, Tokyo Medical University, Tokyo 160-8402, Japan.

Abbreviations used: Ab, antibody; ADAP, adhesion- and degranulation-promoting adapter protein; Ag, antigen; Arp2/3, actin-related protein 2/3; cSMAC, central SMAC; dKD, double knockdown; Erk, extracellular signal–regulated kinase; ICAM, intercellular adhesion molecule; IS, immunological synapse; LAT, linker for activation of T cells; MC, microcluster; MCC, moth cytochrome C; MTOC, microtubule-organizing center; SMAC, supramolecular activation cluster; tg, transgenic; TIRF, total internal reflection fluorescence; WASP, Wiskott-Aldrich syndrome family protein.

The Rockefeller University Press $30.00
J. Exp. Med. 2016 Vol. 213 No. 8 1609–1625
www.jem.org/cgi/doi/10.1084/jem.20151088

and Ostergaard, 2011). Pxn and Pyk2 have also been observed in the microtubule-organizing center (MTOC) and possibly participate in the MTOC relocation and killing function in cytotoxic T cells and NK cells (Herreros et al., 2000; Sancho et al., 2000, 2002; Robertson et al., 2005; Robertson and Ostergaard, 2011). Pyk2 was shown to be involved in CD28 signaling, integrin co-stimulation, and the development of short-lived CD8 effector T cells (van Seventer et al., 1998; Tsuchida et al., 1999; Beinke et al., 2010). However, the molecular basis of the function of focal adhesion molecules in the initial TCR signaling has not yet been elucidated.

Signals from both TCRs and integrin trigger generation of filamentous actin (F-actin) polymer through activation of Wiskott-Aldrich syndrome family proteins (WASPs, WASP family verprolin-homologous proteins [WAVE], etc.) and actin-related protein 2/3 (Arp2/3) complexes (Dustin and Cooper, 2000; Barda-Saad et al., 2005). During IS formation, it has been shown that F-actin polymerization is induced initially at TCR-MCs and particularly supports the recruitment of PLC-γ (Kumari et al., 2015). In later phases, F-actin formed in the marginal area is critical for cell adhesion and lamellipodia formation. F-actin is also essential for promoting the initial movement of newly generated TCR-MCs through actin retrograde flow (Barda-Saad et al., 2005; Campi et al., 2005; Yu et al., 2010). The actin-binding protein nonmuscle myosin II (MyoII) is one of the major players of F-actin–dependent functions. Although its role in T cell function was controversial, T cell motility, assembly and movement of TCR-MCs, and MTOC relocation are regulated by the MyoII-mediated contractility of actin (Jacobelli et al., 2004; Ilani et al., 2009; Liu et al., 2013).

In this study, we discovered a novel structure of adhesion molecules surrounding TCR-MCs that is required for T cell activation, particularly for facilitating activation under weak stimulation. The structure was similar to the IS, although the size was almost 10 times smaller. This ring structure includes LFA-1, Pxn, Pyk2, vinculin, and MyoII, which are supported by F-actin and MyoII activity through LFA-1 outside-in signals. These micro–adhesion rings supported TCR-MC development, especially LAT and SLP76 clustering. Disruption of the micro–adhesion ring by down-regulation of both Pxn and Pyk2 resulted in the impairment of TCR-MC formation, phosphorylation of signal molecules, and IL-2 production. These results indicate that the micro–adhesion ring is essential for T cell activation.

RESULTS

TCR-MCs are transiently bordered by focal adhesion molecules

To analyze the contribution of the LFA-1–mediated outside-in signal in the IS formation and T cell activation, we analyzed LFA-1–related molecules using a planar bilayer containing moth cytochrome C (MCC)–loaded MHC class II I-E^k and ICAM-1. T cells from AND-TCR transgenic (tg) mice were transduced with GFP-labeled molecules and stained with Dylight549 (Dy549)-labeled anti–TCR-β (H57) Fab to visualize the TCR. The images of fluorescence at the interface between the T cell and the bilayer were collected by total internal reflection fluorescence (TIRF) microscopy.

Staining of LFA-1 and TCR on fixed T cells revealed that LFA-1 formed small rings surrounding TCR-MCs (Fig. 1 A). GFP-labeled Pxn (Pxn-GFP) in live T cells showed clearer rings surrounding TCR-MCs (Fig. 1 B, left). The fluorescent intensity profiles of Pxn-GFP and TCRs showed that the fluorescent peaks did not overlap and distributed in an alternating way (Fig. 1 B, middle). The nonoverlapping feature was confirmed by plotting normalized pixel intensities of Pxn-GFP versus TCRs showing low correlation (Fig. 1 B and Fig. 2 C, right). The distribution and dynamics of the rings of Halo tag–labeled Pxn (Pxn-Halo) were almost identical to focal adhesion kinase Pyk2-GFP (Fig. 1 C). The fluorescent intensity profiles of Pyk2-GFP and Pxn-Halo showed their colocalization (Fig. 1 C, middle). The plot of normalized pixel intensities of Pyk2-GFP versus Pxn-Halo revealed a highly positive correlation (Figs. 1 C and 2 C, right). Staining of vinculin on fixed T cells as an endogenous focal adhesion molecule also showed similar rings (Fig. 1 D). Therefore, both integrin and focal adhesion molecules formed the micro–adhesion ring surrounding TCR-MCs. The criteria of the micro–adhesion ring are shown in Fig. 1 F. The concentric arrangement of TCRs and micro–adhesion rings resembles mature ISs in microscale.

Analysis of sequential images of TCR and Pyk2-GFP at the adhesion area revealed that the formation of micro–adhesion rings is transient (Fig. 1 E and Video 1). The generation of micro–adhesion rings began just after the initial TCR-MC formation, and their numbers increased with increasing TCR-MCs. However, these structures disappeared before cSMAC formation. The images of single micro–adhesion rings chronologically depicted and an array illustrating the duration of individual TCR-MCs and micro–adhesion rings showed that the micro–adhesion ring was formed just after TCR-MC generation at a very early phase of activation but soon disappeared (Fig. 1 G).

Synapse-like structures at the interface of T cells and APCs

We confirmed these synapse-like structures in microscale at the interface of T cells and APCs (Fig. 2). T cells expressing SLP76-GFP were incubated with Ag-pulsed B cells and stained with anti–LFA-1 antibody (Ab). The x–y dimensional analysis at the interface revealed complex distributions of SLP76-GFP and LFA-1 (Fig. 2, A and B). In SLP76-GFP–positive cells conjugated with APCs, 45.2 ± 18.2% of the cells showed SLP76-GFP clusters and LFA-1 staining ordered alternately at the interface. The T cells expressing SLP76-GFP without clustering would have ceased the formation of SLP76 clusters because the SLP76 cluster is generated transiently at the very early activation stage (see Fig. 3 G). The number of SLP76 clusters between LFA-1 staining was evaluated. From the fluorescent intensity profiles shown in

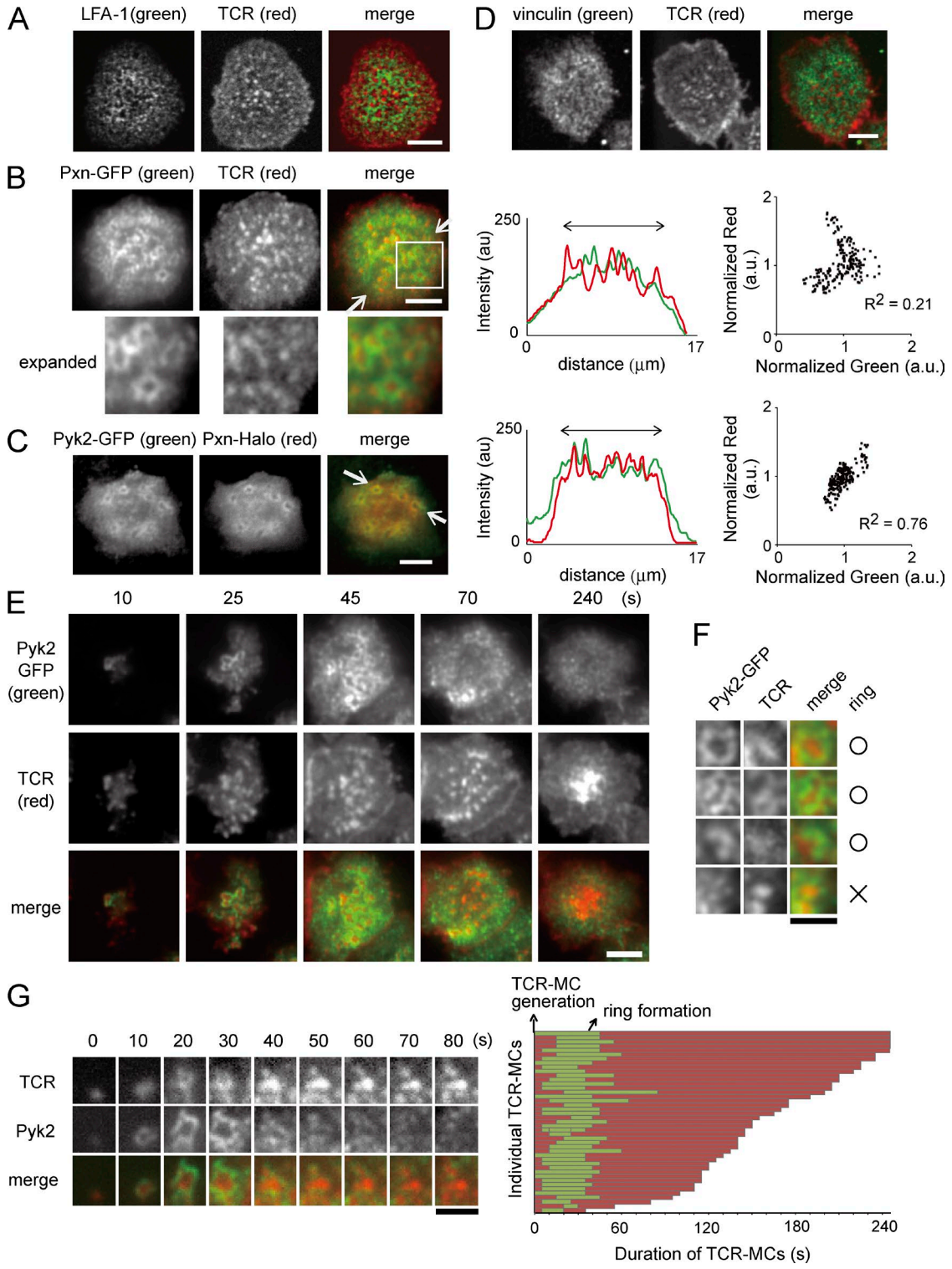

Figure 1. **TCR-MCs in the early phase of activation are bordered with focal adhesion molecules.** (A) T cells were fixed on the planar bilayer, stained with anti-LFA-1–Dy549 and anti-TCR–Alexa Flour 647 Abs, and analyzed with a confocal microscope. Representative images of 58 cells are shown. (B) T cells expressing Pxn-GFP were stained with H57(Fab)-Dy549 (TCR) and analyzed on the planar bilayer by TIRF microscopy. The images at the contact area are shown (top left). For better visualization, the image in the boxed area is shown at higher magnification (bottom left). Representative images of 24 cells are shown. The fluorescent intensity profiles of Pxn-GFP and TCRs between the white arrows are plotted (middle). The pixel intensities of Pxn-GFP and TCRs from 188 pixels in the central area as indicated by the arrows were normalized to their median values and plotted (right). a.u., arbitrary units. (C) T cells

Fig. 2 C (left), the number of SLP76 clusters was estimated as 4.8 ± 2.3 on a diameter and 18.6 ± 9.18 per contact area. The plot of normalized pixel intensities of SLP76-GFP versus LFA-1 from representative cells (middle) was also shown. The means of correlation coefficients of SLP-GFP and LFA-1 from 10 cells were plotted in Fig. 2 C (right). These data clearly showed that SLP76 and LFA-1 were nonoverlapped. As a colocalization positive control, the higher correlation coefficient of Pyk2-GFP and Pxn-Halo was plotted (Fig. 1 C). The lower correlation coefficient of TCR and Pxn-GFP was also plotted for confirmation of similar value from different experimental conditions (Fig. 1 B). We also reconstituted the x–z dimension image and confirmed that SLP76-GFP clusters were surrounded by LFA-1 (Fig. 2 D). These data clearly show that the TCR-MCs in the early phase of activation induce the transient formation of synapse-like structures with micro–adhesion rings.

Apparent formation of micro–adhesion rings and SLP76 clusters by weak stimulation

For quantitative analysis, the number of micro–adhesion rings was counted manually using the criterion explained in Fig. 1 F, whereas the number of TCR-MCs per cell was counted automatically using IMARIS software (BitPlane). First, we analyzed Ag dose dependency of micro–adhesion ring formation (Fig. 3 A and Video 1). The numbers of both micro–adhesion rings and TCR-MCs increased as cellular adhesion progressed, but the number of micro–adhesion rings at the higher doses of Ag (1 and 10 μM) decreased rapidly. In contrast, with lower doses (10 and 100 nM), micro–adhesion rings were generated and sustained for a longer period. Interestingly, whereas the number of TCR-MCs at 10 nM Ag was noticeably reduced, the number of micro–adhesion rings at 10 nM Ag was similar to that of 100 nM Ag. Because the adhesion area was also affected by the strength of TCR stimulation, we evaluated the densities of TCR-MCs and micro–adhesion rings upon stimulation with various Ag doses. The numbers of TCR-MCs or micro–adhesion rings at the peaks were divided by area (square micrometers) and plotted as the density (Fig. 3 B). Interestingly, the densities of TCR-MCs increased as the Ag dose increased, whereas those of micro–adhesion rings were constant except for those with no Ag. Without Ag, 17.4% of added cells showed transient adhesion, but they moved quickly on the bilayer. Consequently, only 1.6% of cells stopped and made a small number of TCR-MCs, which could represent preexisting MCs formed in the absence of Ag as reported previously (Fig. 3, A and C; Crites et al., 2014). Although we found that some of the preexisting MCs were surrounded by micro–adhesion rings (Fig. 3 A), they failed to recruit phosphorylated SLP76 (Fig. 3 D), suggesting that the micro–adhesion rings might not support delivering activation signals in the preexisting MCs. Considering that 10 nM is the minimum Ag dose for T cell stimulation based on the capacity to induce sustained calcium responses and produce IL-2 under this experimental condition (Fig. 3 E), these data suggest that the micro–adhesion ring plays a critical role in supporting T cell activation, particularly upon weak stimulation with low doses of Ag.

We next analyzed the Ag dose dependency in the clustering of ZAP70, LAT, and SLP-76 at TCR-MCs. With 1 μM Ag, all of the ZAP70-GFP, LAT-GFP, and SLP76-GFP formed clear clusters at the TCR-MCs and moved toward the center of the interface with TCR-MCs as previously reported (Fig. 3 F, left; and Video 2; Yokosuka et al., 2005). In contrast, upon stimulation with 10 nM Ag, LAT-GFP and SLP76-GFP formed significant numbers of distinct, clear clusters, but ZAP70-GFP showed only a small number of diffuse, unclear clusters (Fig. 3 F, right). The kinetics of the cluster number per cell was examined (Fig. 3 G). The number of ZAP70-GFP clusters by stimulation with 1 μM Ag initially increased and then decreased gradually and was comparable with that of TCR-MCs, but the number with 10 nM Ag was dramatically reduced. In the case of LAT-GFP, the number of clusters was quite similarly induced to that of ZAP70 upon stimulation with 1 μM Ag, but the number of LAT clusters by stimulation with 10 nM Ag was similar to those with 1 μM Ag. The number of SLP76 clusters by stimulation with 1 μM Ag also initially increased and then decreased more rapidly than those of TCR-MCs, and the number of SLP76 clusters by stimulation with 10 nM Ag was similar to those with 1 μM Ag. The kinetics of cluster intensities showed the difference between ZAP70, LAT, and SLP76-GFP clusters more clearly (Fig. 3 H). With 1 μM Ag, the intensities of TCR-MCs and ZAP70-GFP clusters gradually increased, whereas the SLP76-GFP clusters rapidly disappeared, and LAT-GFP clusters showed the intermediate pattern of ZAP70 and SLP76. TCR-MCs and ZAP70-GFP clusters upon stimulation with 10 nM Ag had much lower intensities than those with 1 μM Ag, whereas SLP76-GFP clusters showed similar intensities throughout the period, and LAT again showed the interme-

expressing both Pyk2-GFP and Pxn-Halo were examined. The representative images of five cells are shown. The fluorescent intensity profiles of Pyk2-GFP and Pxn-Halo between the white arrows are plotted (middle). The pixel intensities of Pyk2-GFP and Pxn-Halo from 188 pixels analyzed the same as in B are plotted (right). (D) Fixed T cells were stained with anti-vinculin–FITC and anti-CD3–Alexa Fluor 647 mAbs and analyzed as in A. Representative images of 58 cells are shown. (E) T cells expressing Pyk2-GFP were similarly analyzed. Sequential images of Pyk2-GFP and TCR are shown in chronological order. Representative cells of 23 cells were selected. (F) Criterion for counting micro–adhesion ring is shown for Pyk2 and TCR images. TCR-MCs surrounded by more than half of their periphery with Pyk2 were counted. In this example, the three images from the top are positive, and the one on the bottom is negative. (G) The images of each individual TCR-MC and Pyk2-GFP ring from the cell shown in E (left) and an array illustrating the duration of 43 TCR-MCs and micro–adhesion rings (right) are shown. Red bars indicate the total lifetime of each TCR-MC, and green bars show the period when it was bordered by the Pyk2-GFP ring indicative of micro–adhesion ring formation. Time 0 means the time point of observed cluster formation. Bars: (A–E) 5 μm; (F and G) 1.5 μm.

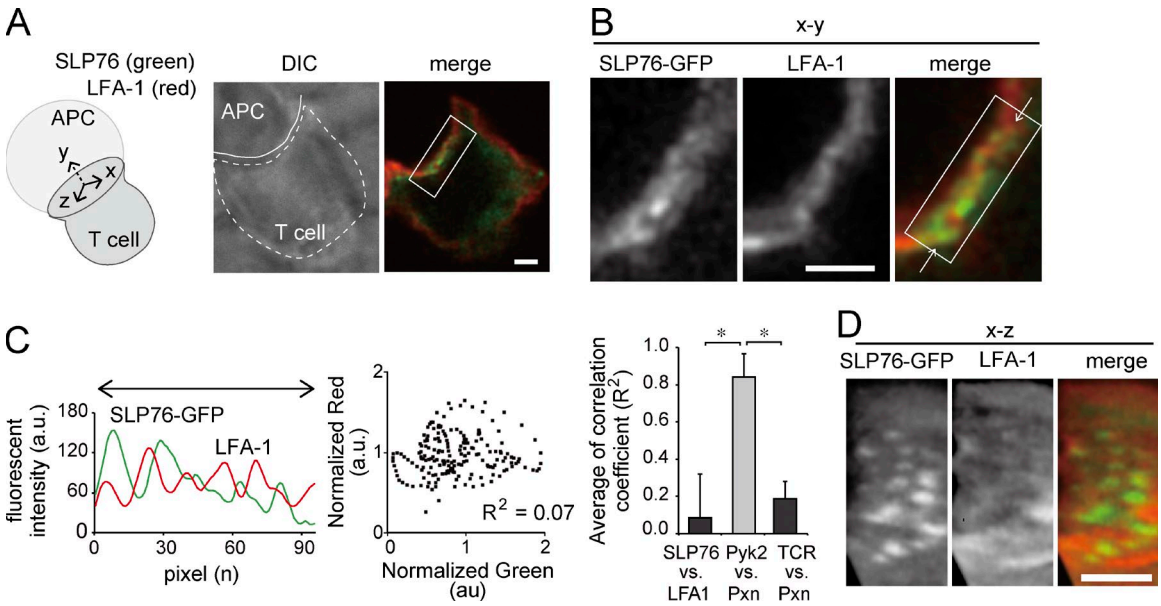

Figure 2. **Micro–adhesion rings at the interface between T cells and APCs.** (A–D) T cells expressing SLP76-GFP were incubated with 1 µM Ag–loaded activated B cells for 5 min and fixed. The images of SLP76-GFP and anti–LFA-1–Dy549 staining are shown. (A) The xyz dimensions are indicated in the diagram (left). The representative images of 14 cells in the x–y dimension are shown (right). DIC, differential interference contrast. (B) The region in the box in A with a higher magnification is shown. (C) The fluorescence intensity profiles of LFA-1 and SLP76-GFP in between the white arrows in B were plotted (left). The pixel intensities of SLP76-GFP and LFA from 189 pixels were normalized to their median values and plotted (middle). The mean of the correlation coefficients of SLP76-GFP and LFA from 10 T cells conjugated with APC was plotted (right). The correlation coefficients of Pyk2-GFP and Pxn-Halo and TCR and Pxn-GFP were also evaluated from the cells analyzed on the planer bilayer shown in Fig. 1 (B and C). Data are the mean from five cells ± SD. *, $P < 0.01$. a.u., arbitrary units. (D) The reconstituted x–z images in the box in B are shown. Bars, 3 µm.

diate pattern of ZAP70 and SLP76. In this analysis, only the clusters generated within 1 min after attachment were analyzed because the clusters may have fused to each other later.

We detected a similar difference in the cluster formation between ZAP70 and SLP76 when using lower affinity Ag (a variant MCC K99A peptide) or T cells expressing low-affinity TCR (5c.c7-TCR tg T cells; unpublished data). These results demonstrate that ZAP70 clusters depend on the strength of TCR stimulation, whereas SLP76 clusters are relatively independent of TCR signal strength, and LAT clusters are formed in both a TCR signal–dependent and –independent fashion. TCR signal–independent LAT clustering and SLP76 clustering were similar to micro–adhesion ring formation. Consistently, almost all of the LAT clusters and SLP76 clusters were at the center of the micro–adhesion ring like small ISs upon 10 nM Ag stimulation (Fig. 3 I).

Formation of micro–adhesion ring depends on LFA-1–mediated outside-in signaling

It has been shown that SLP76 clusters are induced not only by TCR stimulation, but also by the LFA-1–mediated outside-in signal (Baker et al., 2009). Therefore, we modulated the strength of the outside-in signal by changing the concentration of the ligand ICAM-1 on the planar bilayer (Fig. 4 A). The concentration of 200/µm^2 of ICAM-1 was used throughout the study because it is the equivalent level to that on the activated dendritic cells. When the ICAM-1 concentration was decreased to 20/µm^2, the number of micro–adhesion rings was reduced to half, whereas that of TCR-MCs was not changed. With 2/µm^2 of ICAM-1, the micro–adhesion rings were not induced at all, whereas TCR-MCs were still detected, suggesting that the generation of micro–adhesion rings strongly depends on the LFA-1 outside-in signal. The densities of micro–adhesion rings (the number per area) at the peak also decreased by reducing ICAM-1 concentration, whereas those of TCR-MCs were not significantly changed (Fig. 4 B). The number and density of SLP76 clusters by the outside-in signal showed similar results as the micro–adhesion rings (Fig. 4, A and B). Therefore, SLP76 clusters upon stimulation with low-dose Ag would be supported by the micro–adhesion ring. The intensity of TCR-MCs slightly increased with 2/µm^2 of ICAM-1, probably because of the excessive accumulation of TCRs through reduced integrin activation (Fig. 4, C and E). Because the majority of the cells did not adhere to the bilayer with 2/µm^2 of ICAM-1 and only a few cells were adherent and stopped, it may not represent a physiological condition (Fig. 4 D). Nevertheless, even under such conditions, SLP76-GFP clusters with 2/µm^2 of ICAM-1 had significantly lower intensity (Fig. 4 B). These data indicate that micro–adhesion rings depend on LFA-1–mediated outside-in signaling and that SLP76 clusters were predominantly supported by this structure.

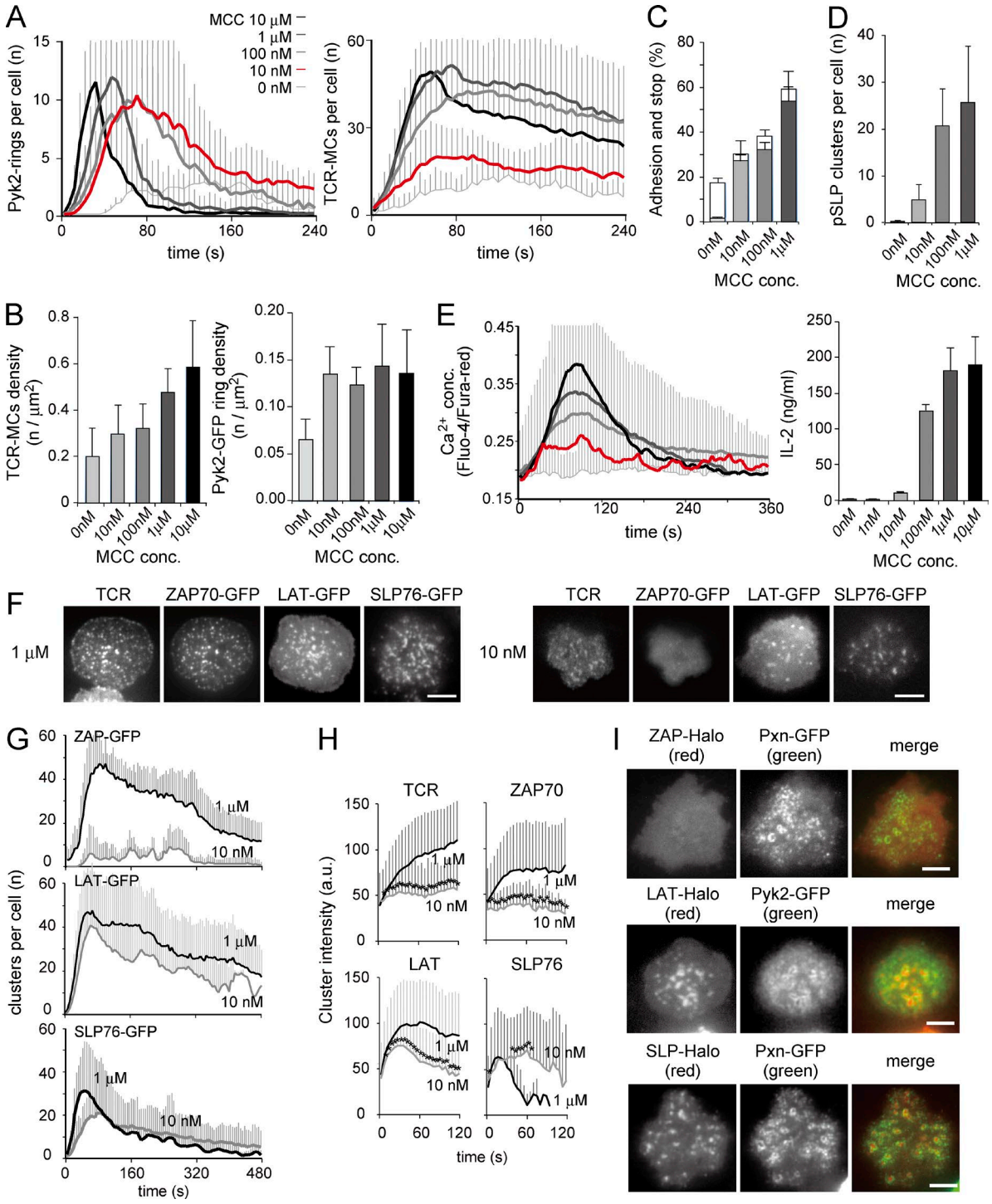

Figure 3. **Apparent formation of micro–adhesion rings and LAT and SLP76 clusters at weak TCR stimulation.** (A) T cells expressing Pyk2-GFP were examined on the planar bilayers. The concentration of loading Ag peptide was changed from 10 nM to 10 μM, and Pyk2-GFP rings and TCR-MCs per cell were counted. (B) Concentrations (conc.) of TCR-MCs and Pyk2-rings at the time point of maximum number for each in A are plotted. (A and B) Data are the mean from 12–24 cells for each condition ± SD. (C) The rates of cells that adhered and moved (shaded bar) or adhered and stopped (unshaded bar) are plotted. Data are the mean from 505–773 cells for each condition ± SD. (D) The number of phosphorylated SLP76 (pSLP) clusters per fixed T cells on the planar bilayers was counted. Data are the mean from 10–24 cells for each condition ± SD. (E, left) T cells were loaded with Fluo-4 and Fura-red and analyzed on the planar bilayers. The ratios of fluorescence intensities of Fluo-4 versus Fura-red were plotted over time. Data are the mean from 64–174 cells for each condition ± SD. (right) T cells were stimulated with the glass beads coated with planar bilayer that was loaded with Ag peptides. IL-2 in the culture

F-actin is essential for micro–adhesion rings and SLP76 clusters

It was shown that adhesion- and degranulation-promoting adapter protein (ADAP) regulates integrin-mediated cell adhesion from both inside-out and outside-in signals by stabilizing the recruitment of WASP to SLP76 for actin rearrangement (Peterson et al., 2001; Baker et al., 2009; Pauker et al., 2011). We confirmed that the SLP76 cluster in T cells from ADAP KO mice was severely reduced in intensity but was intact in number, which was probably supported by intact F-actin clusters (unpublished data). Therefore, we analyzed the contribution of F-actin on micro–adhesion rings.

F-actin distribution was analyzed by using the F-actin–binding peptide Lifeact. Lifeact-GFP was accumulated at TCR-MCs and in the peripheral lamellipodia area upon stimulation with 1 μM Ag, and they showed distinct, clear clusters, even with 10 nM Ag stimulation, which were colocalized with SLP76-GFP clusters and surrounded by Pxn-Halo rings (Fig. 5, A and B; and Video 3). Other F-actin–related molecules, WASP (Fig. 5, A and B) and the Arp2/3 complex (not depicted), were similarly detected at TCR-MCs upon stimulation with 10 nM Ag.

To confirm the importance of F-actin for the synapse-like structure, T cells were acutely treated with cytochalasin D (CytD), which promptly inhibits actin polymerization. CytD was added at the point of maximum spreading, and the time course of micro–adhesion rings and other cluster numbers are shown in Fig. 5 E. Inhibition of actin polymerization was confirmed by the rapid disappearance of Lifeact-GFP clusters after CytD addition (Fig. 5 E, bottom right). TCR-MCs and ZAP70-GFP clusters upon stimulation with 1 μM Ag were not changed by the addition of CytD and remained. These data were consistent with the previous study by Varma et al. (2006) that showed new generation of TCR-MCs was inhibited by F-actin inhibitor, whereas they were resistant to F-actin inhibitor after generation. The adhesion area was also comparable in CytD-treated T cells because CytD was added after the maximum expansion of the T cells (Fig. 5 G). In contrast, SLP76-GFP clusters and LAT-GFP clusters upon stimulation with 1 μM Ag decreased much more rapidly than the control by the addition of CytD. 10 nM Ag was used for Pyk2-GFP because they showed more prolonged micro–adhesion ring formation than with 1 μM Ag. Pyk2-GFP rings and SLP76-GFP clusters upon 10 nM Ag stimulation rapidly disappeared by CytD treatment similar to Lifeact-GFP. The images after the addition of CytD are shown in Fig. 5 F and Video 4.

Furthermore, pretreatment of T cells with Arp2/3 complex inhibitor CK666 (CK) was also used to inhibit F-actin. The T cells treated with 30 μM CK for 30 min dramatically reduced the number of Pyk2-GFP rings (Fig. 5 C), whereas the significant number of TCR-MCs remained, and the intensity of TCR-MCs decreased (Fig. 5 D).

These data clearly show that micro–adhesion rings, LAT clusters, and SLP76 clusters are dependent on F-actin, whereas TCR-MCs and ZAP70 clusters are relatively independent. The components of the synapse-like structure were clearly divided into two types: F-actin–dependent clustering (LAT, SLP76, micro–adhesion ring, etc.) and independent clustering (TCR, ZAP70, etc.).

Micro–adhesion ring formation depends on MyoII activity

Because the micro–adhesion ring is tightly associated and regulated by F-actin, we next examined the involvement of MyoII as an F-actin–related effector molecule for micro–adhesion ring function. T cells expressing Pxn-Halo or SLP76-Halo were loaded with tetramethylrhodamine (TMR) ligand and treated with 50 μM blebbistatin (Blebb), a MyoII inhibitor, for 3 h before micro–adhesion ring formation. Pretreatment with Blebb reduced Pxn-Halo rings and SLP76-Halo clusters, although it significantly retained the numbers and densities of TCR-MCs (Fig. 6 A), suggesting that MyoII activity is strongly related to the micro–adhesion ring formation. The kinetics of the cluster intensities showed that the TCR-MCs were slightly reduced and SLP76-Halo clusters were reduced and shortened (Fig. 6 B). Imaging analysis by using anti-MyoII Ab revealed that MyoII was colocalized with LFA-1 surrounding TCR-MCs (Fig. 6 C).

Therefore, these results suggest that MyoII and its activity are essential for the formation of synapse-like structures, especially for the recruitment of focal adhesion molecules. The impaired micro–adhesion ring would reduce the size of TCR-MCs and F-actin clusters and would result in defects in SLP76 clustering.

Critical role of the micro–adhesion ring for generation of TCR-MCs

To investigate the importance of the micro–adhesion rings for TCR-MCs and T cell activation, RNA interference with shRNA for focal adhesion molecules was used. T cells were retrovirally transduced with shRNA for control (shCtrl), Pxn (shPxn), and Pyk2 (shPyk2). Down-regulation of Pxn and Pyk2 expression was confirmed by Western blotting (Fig. 7 A). The shCtrl-, shPxn-, and shPyk2-trans-

supernatants from 10^5 cells at 24 h was measured by ELISA. Data are representative of three independent experiments. (F) T cells expressing ZAP70-GFP, LAT-GFP, or SLP76-GFP were analyzed on the planer bilayer. Representative images of 20–36 cells at the maximum cell spreading time are shown. (G) The cluster numbers of ZAP70-GFP, LAT-GFP, and SLP76-GFP per cell are plotted over time. Data are the mean from 20–36 cells ± SD. (H) The mean intensities of individual clusters generated during the initial 1 min in G are plotted per time. Data are the mean from 163–272 clusters ± SD. *, $P < 0.01$. a.u., arbitrary units. (I) T cells expressing both ZAP70-Halo and Pxn-GFP (top), LAT-Halo and Pyk2-GFP (middle), or SLP76-Halo and Pxn-GFP (bottom) were examined on the planar bilayers with 10 nM Ag. Representative images of 16–36 cells at the time of maximum cell spreading are shown. Bars, 5 μm.

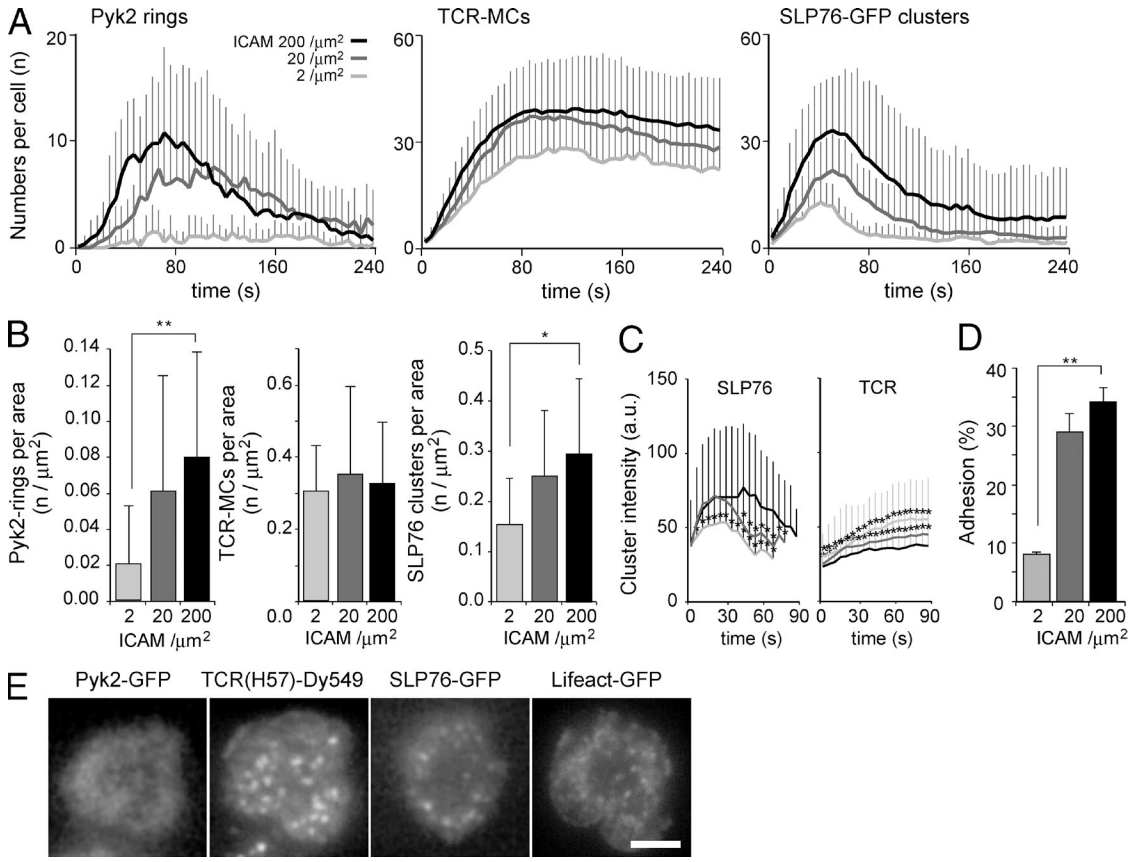

Figure 4. **Micro–adhesion ring formation is dependent on integrin outside-in signal.** (A) T cells expressing Pyk2-GFP or SLP76-GFP were examined on the planar bilayers containing 200, 20, or 2/μm² of ICAM-1. The numbers of TCR-MCs, Pyk2-GFP rings, and SLP76-GFP clusters per cell are plotted. Data are the mean from 16–29 cells for each condition ± SD. (B) The mean concentrations of Pyk2-GFP rings, TCR-MCs, and SLP76 clusters at the peak of numbers of TCR-MCs in A ± SD are plotted. *, $P < 0.05$; **, $P < 0.01$. (C) The mean intensities of individual TCR and SLP76-GFP clusters generated during the initial 1 min are plotted over time. Data are the mean from 298–447 clusters ± SD. *, $P < 0.01$. a.u., arbitrary units. (D) The rates of cells that adhered and stopped on the planar bilayer with each concentration of Ag peptides are plotted. Data are mean ± SD from 443–752 cells. **, $P < 0.01$. (E) Representative images of Pyk2-GFP, TCR, SLP76-GFP, and Lifeact-GFP on the planar bilayers containing 2/μm² ICAM-1 are shown. Bar, 5 μm.

duced cells on planar bilayers showed no significant difference in TCR-MC numbers upon stimulation with 1 μM Ag (Fig. 7 B). However, the cells cotransduced with shRNAs for Pxn and Pyk2 (double knockdown [dKD] cells) showed an increased number of TCR-MCs and impaired cSMAC formation (Fig. 7, B and C; and Video 5). dKD cells became more mobile on the planar membrane by stimulation with 1 μM Ag than shCtrl cells (Fig. 7 D). This unstable contact of dKD cells would be the reason for the impaired cSMAC formation. When T cells were stimulated with 10 nM Ag, the numbers of TCR-MCs in shPxn and dKD cells were dramatically reduced compared with that in shCtrl cells (Fig. 7 B and Video 5). The reduction in numbers appeared to depend on the size of the adhesion area because the density of clusters was not changed, suggesting that the effect might be based on dysregulation of focal adhesion (Fig. 7 E). Indeed, as expected, in the dKD cells, the number and size of each micro–adhesion ring detected by vinculin staining were decreased (Fig. 7 F).

Analyses of individual clusters revealed that the intensities of TCR-MCs in the dKD cells significantly decreased with both 1 μM and 10 nM Ag (Fig. 7 G). The Lifeact-GFP intensity in the dKD cells was also significantly decreased (Fig. 7 H). The phosphorylation status was analyzed at TCR-MCs by Ab staining. The numbers and intensities of the clusters of phospho-CD3ζ and phospho-SLP76 were decreased in the dKD cells (Fig. 7 I). These data indicate that the development of individual TCR-MCs and the signaling through TCR-MCs including phosphorylation and recruitment of SLP76 are supported by the micro–adhesion ring through regulation of cell adhesion.

Impaired T cell functions by down-modulation of micro–adhesion ring components

To analyze the function of the synapse-like structure, dKD cells were stimulated with Ag peptide/APC, and T cell responses were analyzed. Upon interaction with APC, the frequency of cell adhesion and cSMAC formation was reduced

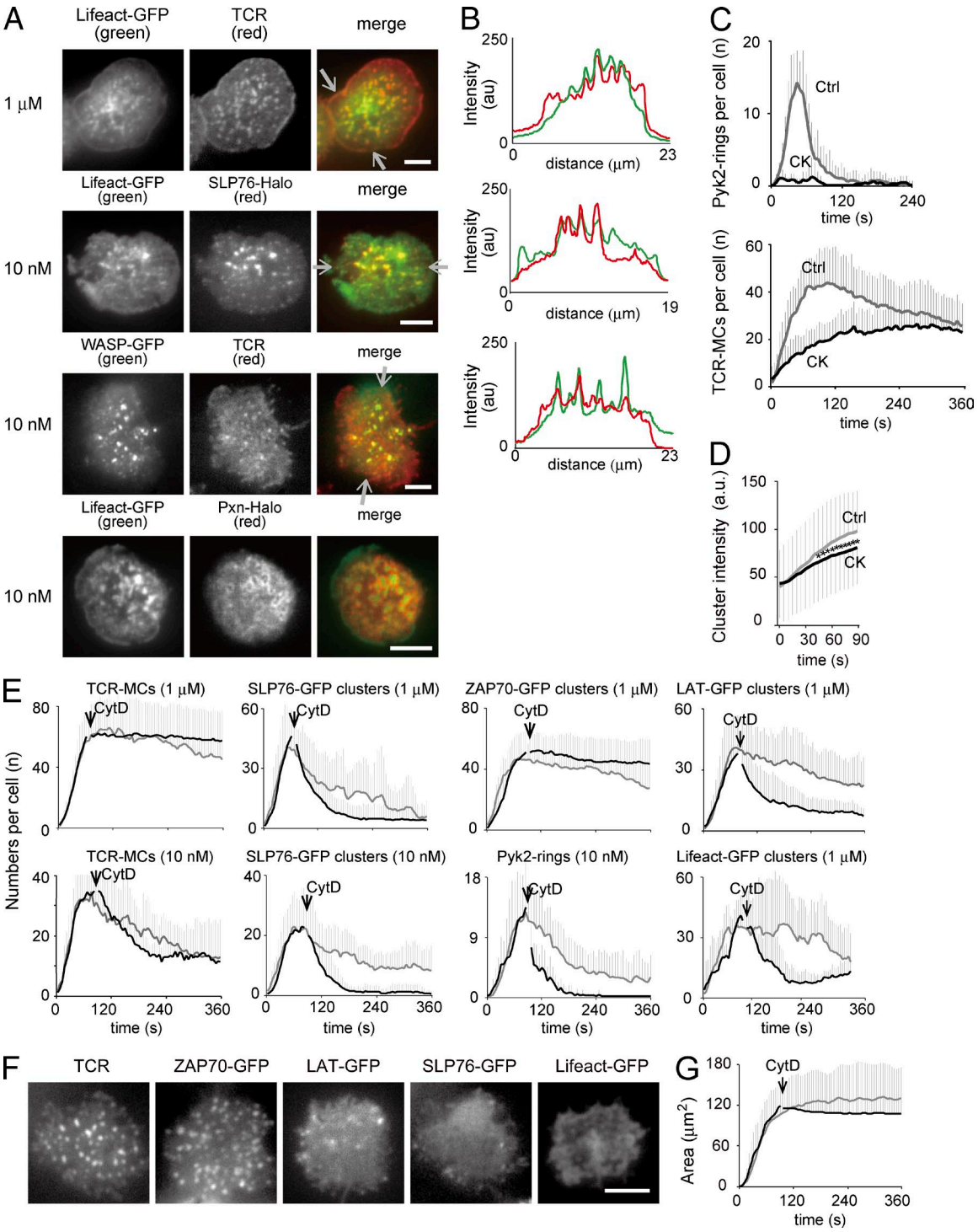

Figure 5. **Dependency of synapse-like structures on F-actin.** (A) T cells expressing Lifeact-GFP, Lifeact-GFP and SLP76-Halo, WASP-GFP, or Lifeact-GFP and Pxn-Halo were examined with 1 μM or 10 nM Ag. Representative images of 8–32 cells are shown. (B) The fluorescence intensity profiles of Lifeact-GFP (green) and TCR (red; top), Lifeact-GFP (green) and SLP76-Halo (red; middle), and WASP-GFP (green) and TCR (red; bottom) in between each pair of white arrows in A are plotted. (C) T cells expressing Pyk2-GFP were pretreated with 30 μM CK666 for 30 min and examined. The numbers of Pyk2 rings and TCR-MCs with (black line) and without (gray line) CK666 treatment are plotted per time. Data are the mean from 14 or 16 cells ± SD. Ctrl, control. (D) The mean intensities of individual TCR clusters generated during the initial 1 min in F are plotted. Data are the mean from 1,309–1,994 clusters ± SD. *, $P < 0.01$. (E) When the T cells expressing Pyk2-GFP, SLP76-GFP, ZAP70-GFP, LAT-GFP, or Lifeact-GFP had expanded on the planar bilayers with 10 nM or 1 μM Ag, CytD was added at a final concentration of 10 μM. The numbers of rings or clusters for each molecule with (black line) and without (gray line) CytD treatment

in dKD cells (Fig. 8 A and Video 6). Consequently, flow cytometric analysis showed that phosphorylation of SLP76 and extracellular signal–regulated kinase (Erk [pErk]) upon stimulation with Ag peptide/APC was reduced in dKD cells (Fig. 8 B). IL-2 production upon stimulation with Ag peptide/APC was significantly reduced in dKD cells, whereas there was no difference even in dKD cells when stimulated by immobilized anti-CD3/CD28 Abs. Unlike molecular assembly and phosphorylation as early signaling, because IL-2 production is a late response, the reduction might be affected by reduced Pyk2/Pxn during a long period in addition to defective micro–adhesion rings (Fig. 8 C).

To determine the functional importance of the synapse-like structure further, we tried to dissect TCR and LFA-1 stimulation by using lipid bilayer–coated glass beads. We used three types of lipid bilayer–coated beads: only I-E^k–coated beads (E^k), both I-E^k– and ICAM-1–coated beads ([E^k + ICAM]), and a mixture of I-E^k beads and ICAM-1 beads ([E^k] + [ICAM]; Fig. 8 D, top). shRNA-treated T cells were stimulated by these glass beads with 1 μM Ag peptides, and the level of pErk as the representative activation signal was analyzed (Fig. 8 D). shCtrl cells stimulated with [E^k + ICAM] showed an increased level of pErk compared with those stimulated with E^k, demonstrating that ICAM-1 enhances pErk. In contrast, in shCtrl cells stimulated with [E^k] + [ICAM] separately, the level of pErk was almost comparable with those stimulated with E^k alone, suggesting that the ICAM-1 stimulation apart from I-E^k had little effect on T cell activation. The significance of the close proximity between I-E^k and ICAM-1 for T cell activation is consistent with and supports our idea that the synapse-like structure micro–adhesion ring surrounding TCR-MCs is critical for initial TCR signals. In contrast, the pErk induction upon stimulation with [E^k + ICAM] was much lower in dKD cells than that in shCtrl cells and was not significantly changed from that with [E^k] + [ICAM] (Fig. 8 D). The proportion of pErk-positive cells was counted, and the statistical results were plotted in Fig. 8 E (left). The same results were obtained in nontransfected CD4 T cells (Fig. 8 E, right). These results suggest that dKD cells could not be fully activated by [E^k + ICAM], probably because of the lack of close proximity of TCR and LFA-1 by the defect in micro–adhesion ring formation around TCR-MCs.

DISCUSSION

In this study, we describe the discovery of a specific structure of micro–adhesion rings just around TCR-MCs, which is required for early T cell activation (Fig. 8 F). The micro–adhesion ring is composed of integrin, focal adhesion molecules, and MyoII and surrounds each TCR-MC. Considering that the mature IS is composed of centralized TCRs and surrounding LFA-1, this structure resembles the IS in microscale, which we may call a microsynapse. The formation of the synapse-like structure is transient during the early stage of T cell activation and depends on LFA-1–mediated outside-in signals, F-actin, and MyoII activity. The micro–adhesion ring plays a critical role in facilitating adhesion, TCR clustering, and F-actin cluster formation to recruit LAT and SLP76 and generating TCR signals. Such function of the synapse-like structure to amplify and support TCR activation was particularly obvious upon weak stimulation with low doses of Ag.

It has been previously reported that LFA-1 induces dot clusters separately from TCR-MCs during the initial phase of T cell activation (Kaizuka et al., 2007). In the present study, we showed that LFA-1 was transiently accumulated to form a ring structure surrounding TCR-MCs. The ring structure was more clearly observed by Pxn-GFP or Pyk2-GFP than by CD11a-GFP (unpublished data), probably because of the abundant expression of CD11a-GFP on the cell surface. Indeed, more LFA-1 rings were detected by anti–LFA-1 staining than CD11a-GFP overexpression. Therefore, the number of the micro–adhesion rings identified by the transfected Pxn-GFP or Pyk2-GFP might be an underestimate of the total number.

The micro–adhesion ring has some similarities to the podosome/invadosome. The podosome is a cylindrical structure formed in a vertical direction on the ventral cell surface to support invasion of cancer cells or dendritic cells (Murphy and Courtneidge, 2011). The similarities include molecular components, size, dependency on receptor stimulation, outside-in signaling, MyoII activity, and structure with an F-actin core surrounded by adhesion molecules. (Collin et al., 2008; Albiges-Rizo et al., 2009; van den Dries et al., 2013). There has been a study describing a podosome-like protrusion at the interface between T cells and epithelial cells or APCs (Sage et al., 2012). This structure contained TCR, F-actin, and ZAP70, and the authors suggested its role in invading the carbohydrate forest on APC to find the peptide–MHC complex on the cell surface. Because the micro–adhesion rings are formed transiently during the early stage of T cell activation and are involved in the initial cell adhesion and activation, they may be similar to the podosome-like structure. Although we failed to detect such a small protrusion in T cells on the planar bilayer system using electron microscopy in our previous study (Hashimoto-Tane et al., 2011), the structural characterization of the observed synapse-like structure remains to be analyzed.

Because there is no means of specific disruption of the micro–adhesion ring to help determine its function, we analyzed T cell function after down-regulating two components of the micro–adhesion ring, Pxn and Pyk2. Consistent with a previous study of Pyk2 KO mice (Beinke et al., 2010), shPyk2

are plotted per time. Arrows indicate the kinetics of CytD addition. Data are the mean from 12–18 cells ± SD. (F) Representative images of TCR, ZAP70-GFP, LAT-GFP, SLP76-GFP, and Lifeact-GFP at 90 s after the addition of CytD are shown. (G) The mean contact area with and without CytD treatment is plotted over time. Data are the mean from 16 cells ± SD. a.u., arbitrary units. Bars, 5 μm.

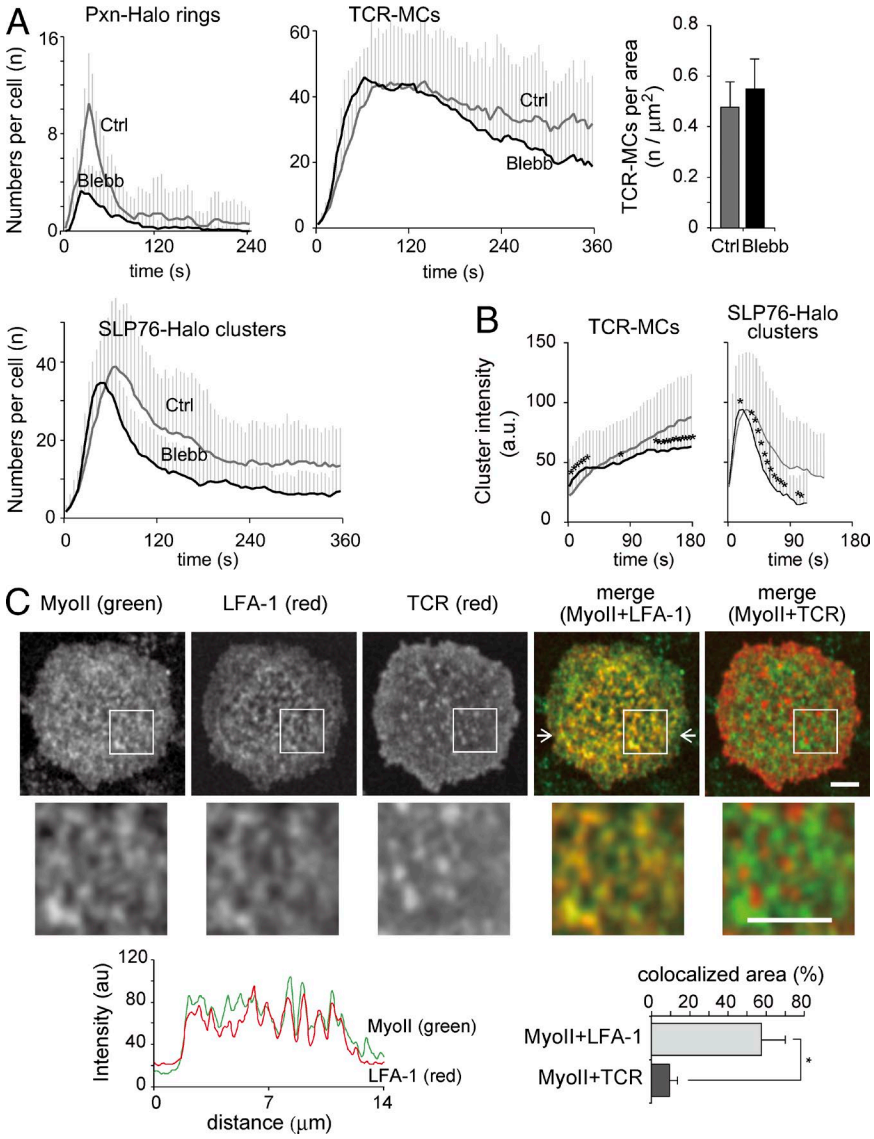

Figure 6. **Micro–adhesion ring formation is dependent on MyoII activity.** (A–C) T cells expressing Pxn-Halo or SLP76-Halo were pretreated with 50 μM Blebb for 3 h and examined on the planar bilayers. (A) The numbers of clusters with (black line) and without (gray line) Blebb treatment are plotted over time. Data are the mean from 12–16 cells ± SD (left and middle). The mean concentration of TCR-MCs at the peak of cluster numbers with (black bar) and without (gray bar) Blebb treatment is plotted (right). Ctrl, control. (B) The mean intensities of individual clusters of TCRs or SLP76 generated during the initial 1 min with (black line) and without (gray line) Blebb treatment analyzed in A are plotted. Data are the mean from 416–540 clusters ± SD. *, $P < 0.01$. a.u., arbitrary units. (C) T cells were fixed at 2 min and stained with anti–MyoII-FITC, anti–LFA-1 (CD11a)–Dy549, and anti-CD3(TCR)–Alexa Fluor 647 (top). For better visualization, the images in the boxed areas are shown at a higher magnification (middle). Representative images of 12 cells are shown. The fluorescence intensity profiles of MyoII-FITC (green) and LFA-1 (CD11a)–Dy549 in between the white arrows in the top image are plotted (bottom left). The percentages of MyoII cluster area colocalized with LFA-1 or with TCRs as a control to the total MyoII cluster area were plotted (bottom right). Bars, 3 μm. Data are the mean from 12 cells ± SD. *, $P < 0.01$.

cells showed no structural and functional impairment. In contrast, the Pxn KO mice resulted in early lethality. It may have a role in growth and/or survival of cells, which is consistent with our data that a considerable proportion of shPxn cells failed to grow. Whereas the shPxn T cells had no detectable defects in adhesion or IS formation upon strong stimulation with 1 μM Ag, they showed some defects in cell adhesion and formation of TCR-MCs upon weak stimulation with 10 nM Ag. In contrast, the dKD cells exhibited severely impaired regulation of adhesion, TCR-MC formation, phosphorylation of signaling molecules, and cytokine production. Therefore, it is likely that the function of the micro–adhesion ring primarily depends on Pxn rather than Pyk2, and synergistic effects were observed by double deficiency of both Pxn and Pyk2 for the early stage of T cell activation.

The reduced size of TCR-MCs and impaired TCR proximal signaling were caused by the alteration of micro–adhesion rings. In addition, the defect in cell adhesion in dKD cells upon weak stimulation was also explained by impaired micro–adhesion ring formation because usually adhesion starts from the point of the initial TCR-MC and the generation and maturation of TCR-MCs depends on adhesion rings. In contrast, the increased adhesion area in dKD cells upon strong stimulation may reflect the effects from the general function of focal adhesions; stable adhesion in sessile cells and active cells move by recycling in moving cells (Webb et al., 2004). The dKD cells upon strong stimulation could induce adhesion but also failed to stop cells with narrowing down the adhesion area. The reduced IL-2 production could be mainly caused by the defective initial activation signal but may also be affected by the lack of Pxn or Pyk2 later during the 24-h culture period. The reduced sensitivity of T cell activation in the dKD cells was similarly observed in LFA-1–deficient T cells (Wang et al., 2008), which is consistent with impaired LFA-1 signaling in the dKD cells.

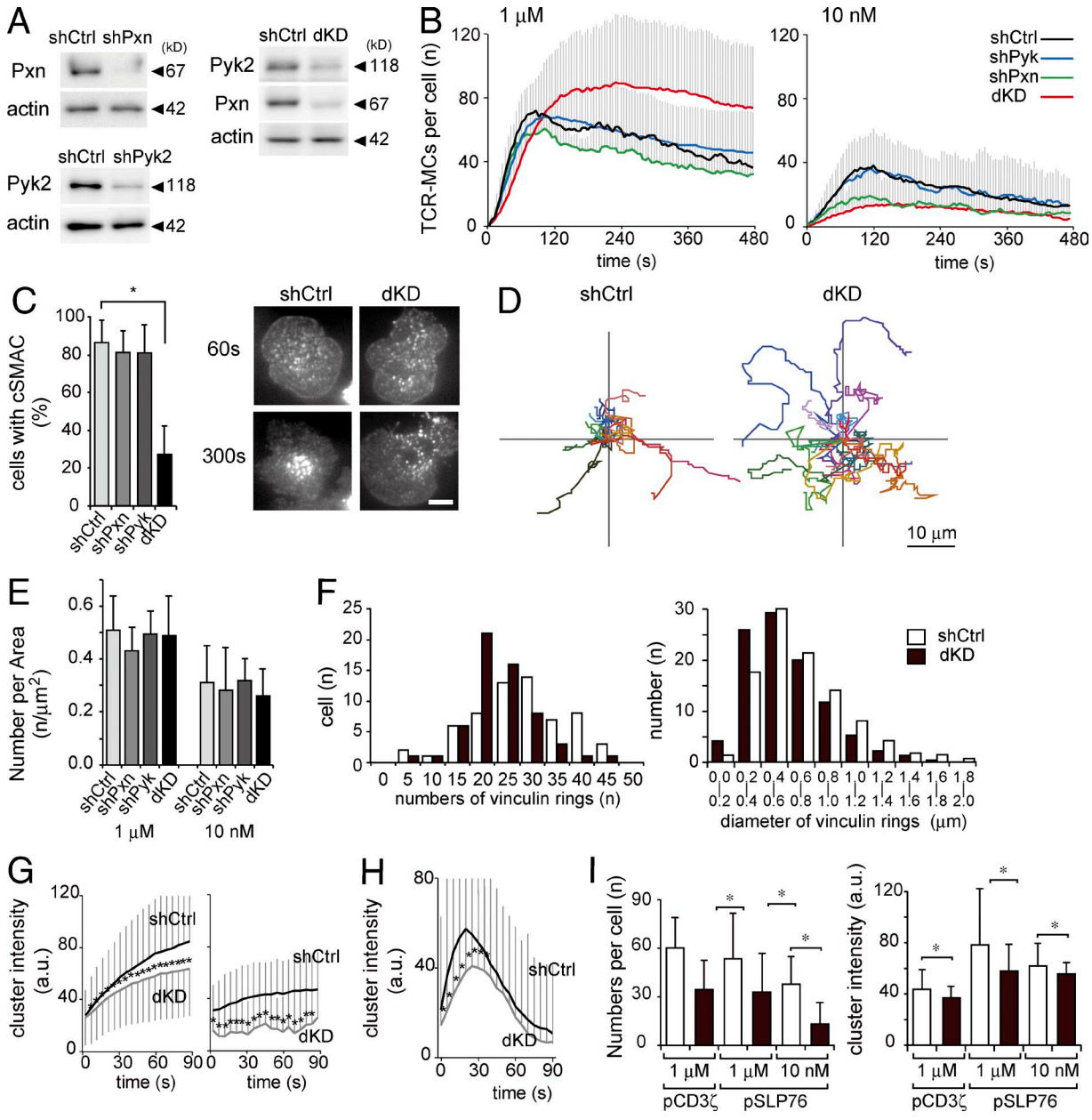

Figure 7. **Critical role of the micro–adhesion ring for TCR-MC development.** (A–I) T cells transduced with shCtrl, shPxn, shPyk2, or shPxn + shPyk2 (dKD) were examined on the planer bilayer. (A) The expression levels of Pxn and Pyk2 with shCtrl, shPxn, shPyk2, or dKD cells were examined by Western blotting. Representative data from three independent experiments are shown. (B) The numbers of TCR-MCs per cell in shCtrl, shPxn, shPyk2, or dKD cells on 1 μM or 10 nM Ag are plotted. Data are the mean from 18–38 cells ± SD. (C) The rates of cells with cSMACs at 10 min on 1 μM Ag–loaded bilayer were plotted (left). Data are the mean from 87–132 cells ± SD. Representative images are shown (right). Bar, 5 μm. (D) The trajectories of movements of shCtrl or dKD cells on 1 μM Ag for 10 min are shown. 16 cells for each condition were analyzed. (E) The concentrations of TCR-MCs in the cells analyzed in B are plotted. Data are the mean from 18–38 cells ± SD. (F) The shCtrl or dKD cells were fixed at 1.5 min and stained with anti-vinculin–FITC mAb. Histograms of the numbers of vinculin rings per cell and the diameters of each ring in shCtrl and dKD cells are shown. Data are from 24 cells for each condition. (G) The mean intensities of individual TCR-MCs in the cells in B are plotted over time. Data are the mean from 526–1,774 clusters ± SD. a.u., arbitrary units. (H) The intensities of individual Lifeact-GFP clusters in shCtrl and dKD cells with 1 μM Ag are shown. Data are the mean of 641 and 635 clusters ± SD, respectively. (I) The mean number of clusters per cell and individual intensities of phospho–CD3-ζ clusters and phospho-SLP76 (pSLP76) clusters in shCtrl (unshaded bars) or dKD (shaded bars) cells is depicted. Data are the mean from 1,098–1,438 clusters ± SD. *, $P < 0.01$.

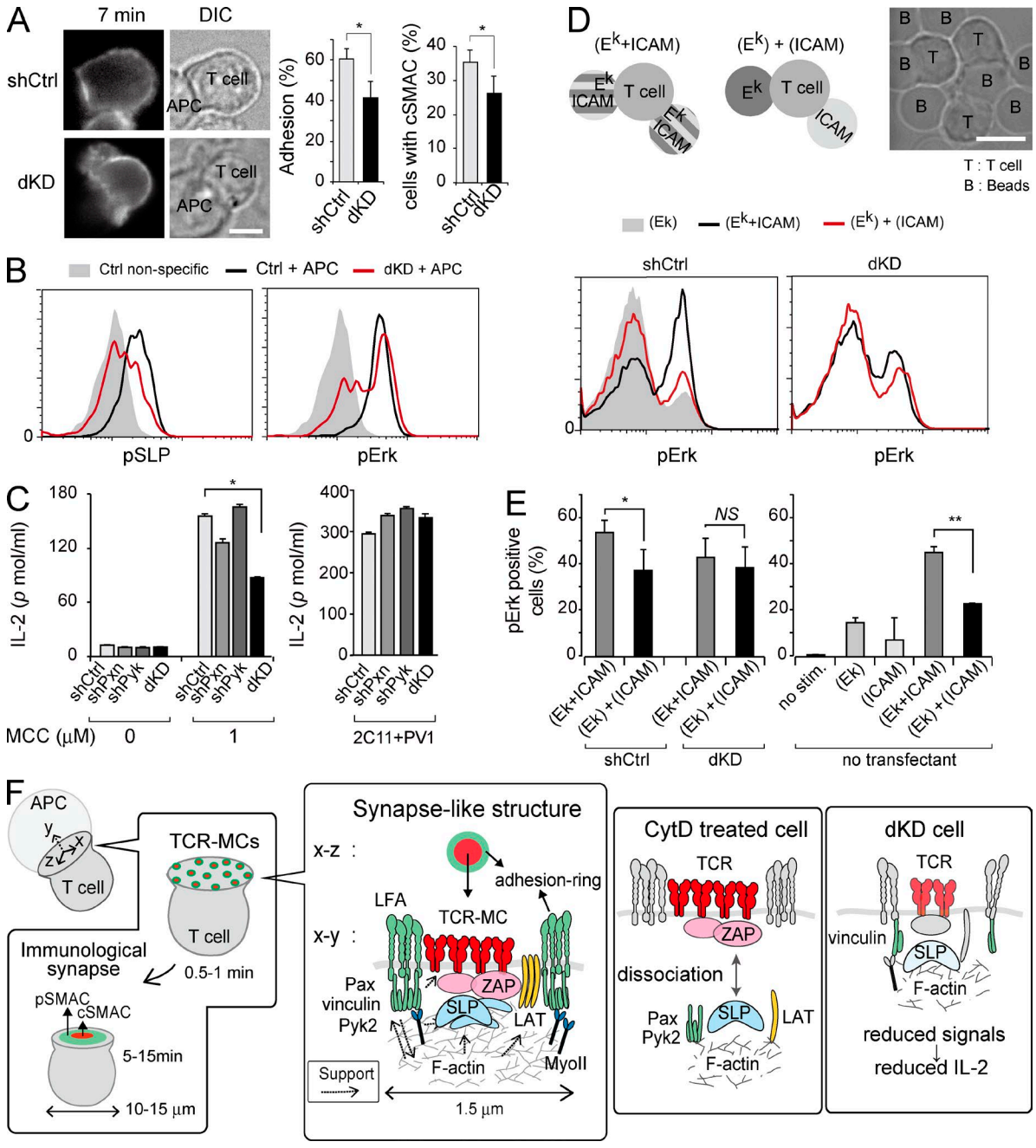

Figure 8. **Impaired T cell functions after down modulation of focal adhesion molecules.** (A) Representative images of the TCR (H57-Dy549) on shCtrl or shPxn + shPyk2 (dKD) cells stimulated with 1 μM Ag–loaded activated B cells are displayed (left). The frequencies of adhered and stopped cells upon interaction with APCs and the rate of the cells with cSMACs after 10 min in the adhered and stopped cells are plotted (right). Data are the mean from 59 or 65 cells ± SD. *, $P < 0.05$. DIC, differential interference contrast. (B) The shCtrl and dKD cells incubated with 1 μM Ag–loaded activated B cells for 10 min were fixed and analyzed for the phosphorylation levels of SLP76 and Erk by flow cytometry. Representative results from four experiments are shown. pSLP, phosphorylated SLP76. (C) The shCtrl, shPxn, shPyk2, and dKD cells were incubated with irradiated spleen cells at the indicated dose of Ag. IL-2 in the culture supernatant after 24 h was measured by ELISA. Representative results from three experiments are shown. Data are mean ± SD. *, $P < 0.01$. (D) T cell stimulation with lipid bilayer–coated beads. Three types of lipid bilayer–coated beads were used: I-E^k coated, both I-E^k and ICAM-1 coated, and a mixture of I-E^k and ICAM-1 coated. The shCtrl and dKD cells were stimulated with the glass beads with 1 μM Ag peptides for 10 min and analyzed for phosphorylation levels of Erk as in C. (E) The nontransfected cells were activated with ICAM-1, E^k, [E^k + ICAM], or [E^k] + [ICAM]. The proportions of pErk-positive cells from shRNA-treated cells in D and nontransfected cells are plotted. Data are the mean of four experiments ± SD. *, $P < 0.05$; **, $P < 0.01$. (F) Diagram of micro–adhesion rings and ISs (pSMAC, peripheral SMAC; left). When a T cell recognizes an Ag on an APC, TCR-MCs are generated at the interface and initiate activation signals. Then, TCR-MCs move to form cSMACs and generate a typical IS. The TCR-MCs in initial phase were surrounded by a micro–adhesion ring;

The colocalization of Pxn and Pyk2 suggested their cooperation at the micro–adhesion ring. According to previous studies (Rodríguez-Fernández et al., 1999; Herreros et al., 2000), it is possible that the cooperation of Pxn and Pyk2 at the MTOC regulates T cell polarization and activation. Indeed, we confirmed reduced efficiency of MTOC translocation in the dKD cells (unpublished data). However, the defects in MTOC translocation could also be explained by the defects in the initial T cell activation. Because the defective processes such as TCR-MC generation and phosphorylation of SLP76 clusters were very early membrane-proximal events, we suggest that the appropriate spatiotemporal generation of micro–adhesion rings with Pxn and Pyk2 is critical for inducing integrin outside-in signals required for T cell activation.

The discovery of the TCR-MC as the responsible structure and the site for inducing initial TCR activation signals revealed that TCR, ZAP-70, LAT, and SLP76 formed a TCR-MC, and their assembly and dynamics upon Ag stimulation were thought to be stoichiometric. However, in the present study, we showed that although the dynamics of TCR and ZAP-70 were almost identical, LAT and SLP76 behaved differently in terms of the kinetics of cluster numbers and intensities and the effects of an actin inhibitor, particularly upon weak TCR stimulation. Interestingly, the transient recruitment of SLP76 to TCRs in the very early phase of activation had also been shown in recent proteome analysis (Roncagalli et al., 2014). Whereas cluster formation of TCRs and ZAP70 was dependent on the strength of the activation signal, LAT and SLP76 clusters were formed relatively independently of signal strength. The observed difference in the dynamics of the LAT and SLP76 clustering from TCRs and ZAP70 was caused by its dependency on the formation of the micro–adhesion ring through LFA-1–mediated outside-in signals and F-actin. Recently, WASP-mediated F-actin–dependent clustering of phospho–PLC-γ was reported (Kumari et al., 2015). The F-actin supporting phospho–PLC-γ as actin foci is similar to the F-actin localized at the core of the synapse-like structure that supports SLP76 clusters and the micro–adhesion ring. Because the characteristics of the phospho–PLC-γ clusters were mostly consistent with LFA-1–mediated SLP76 clusters, it is likely that the PLC-γ clusters would also be under the regulation of the micro–adhesion ring.

In this study, we found the synapse-like structure micro–adhesion ring surrounding TCR-MCs and showed its importance in T cell activation. The adhesion-mediated positive regulation of TCR activation signals was clearly visualized. Such regulation of adhesion and the cytoskeleton will become more important in understanding the signaling and function of T cells.

MATERIALS AND METHODS

Mice. AND-TCR tg mice were provided by S.M. Hedrick (University of California, San Diego, San Diego, CA) by courtesy of R.N. Germain (National Institutes of Health), and 5c.c7 tg mice were provided by M.M. Davis (Stanford University, Stanford, CA). ADAP-deficient mice were provided by G. Koretzky (Weill Cornell Medical College, New York, NY). C57BL/6 and B10.BR mice were purchased from CLEA Japan, Inc. and Japan SLC Inc., respectively. All mice were maintained in our animal facility in specific pathogen-free conditions and treated in accordance with the ethical guidance of the RIKEN Yokohama Institute.

Cell culture. T cells from the spleen and lymph node of AND-tg mice were isolated and purified by using CD4 (L3T4) MicroBeads (Miltenyi Biotec). The purified T cells were stimulated with irradiated spleen cells from B10.BR mice pulsed with 3 μM MCC mutant (MCC(88-103) K99A) peptide (MCC(K99A)) in RPMI 1640 (Sigma-Aldrich) with 10% FBS and 1% penicillin–streptomycin (Invitrogen). The next day, the genes of interest were transduced using a retrovirus-mediated gene transfer system. On day 4, the infected cells were sorted using a flow cytometer (FACS Aria; BD). Fluorescent imaging experiments were performed on the fifth or sixth day of culture. For shRNA treatment, the cells were restimulated with irradiated spleen and MCC(K99A) on the fifth or sixth day, transduced again with virus supernatants on the sixth or seventh day, and subjected to imaging and functional analysis on the 10th to 12th day of culture.

Construction and transduction. All the expression vectors were made by PCR subcloning. The retrovirus vector pMXs (provided by T. Kitamura, Tokyo University, Tokyo, Japan) were used for expression of fluorescent-labeled molecules. ZAP70, SLP76, ADAP, WASP, p16, Arp3, CapZ, Pyk2, Pxn, and CD11a were cloned from complementary DNA of activated AND-tg T cells. GFP was derived from plasmid enhanced GFP–N1 (BD), HaloTag from HaloTag pHT2 vector

this structure resembles mature ISs as the synapse-like structure in microscale. Our results revealed the following scenario. The integrin outside-in signal–induced micro–adhesion ring formation was composed of LFA-1, Pxn (Pax), Pyk2, vinculin, and MyoII. The micro–adhesion ring enhanced F-actin formation and TCR clustering, especially under weak TCR stimulation. (Middle) When F-actin was acutely broken by CytD treatment after TCR-MC generation, TCR-MCs and ZAP70 clusters remained, but the micro–adhesion ring and LAT and SLP76 clusters disappeared. However, when F-actin formation was inhibited before TCR-MC generation by CK666 treatment, the generation of both TCR-MCs and micro–adhesion rings was inhibited. Therefore, F-actin is important for both generation and maintenance of the TCR-MC signaling. (Right) In the dKD (shPxn + shPyk2) cells, the decrease of focal adhesion molecules caused defects in micro–adhesion ring formation. Consequently, small TCR-MCs and F-actin clusters were formed, and T cell activation such as phosphorylation of SLP76 and Erk and IL-2 production was impaired. (A and D) Bars, 5 μm.

(Promega), and Lifeact from Lifeact-TagRFP2 pCMV (ibidi). The pMSCV-LTRmiR30-PIG(LMP) retrovirus vector (GE Healthcare) was used for shRNA expression. We used several different markers to detect doubly transduced cells. In addition to GFP, CD8 without the cytoplasmic region was used for shPxn or shCtrl, and rat CD2 without the cytoplasmic region was used for shPyk2 by inserting them after the internal ribosomal entry site. The sequences used were shPxn, 5′-CCCCTGGTGAAAGAGAAGCCAA-3′; shPyk2, 5′-AAGAAGTAGTTCTTAACCGCAT-3′; and shCtrl, 5′-GCACGGGGAAGGAGCGGGAA-3′. To produce pseudovirus, the recombinant plasmids were transfected into Phoenix packaging cells (G. Nolan, Stanford University, Stanford, CA) using Lipofectamine 2000 (Invitrogen).

Abs. For live imaging of TCR, the Fab fragment of anti–TCR-β Ab (H57) was labeled with Dylight549. anti-Pxn Ab (BD610051) and anti-Pyk2 Ab (D-1; sc-365201) were used for Western blotting. For immunohistochemistry, anti–CD3-ε Ab labeled with Alexa Flour 647 (BD557889), anti-vinculin Ab (F7053; Sigma-Aldrich), anti–LFA-1 Ab (H155-78; BioLegend) labeled with Dylight 549, and anti-MyoII Ab labeled with FITC (orb4013) were used. For FACS analysis, anti–phospho-Erk Ab (Phosflow 812593; BD) and anti–phospho-SLP76 Ab labeled with APCs (Phosflow 558438; BD) were used.

Planar bilayer system. Glycophosphatidylinositol (GPI)-anchored mouse MHC class II I-E^k and ICAM-1 were purified as previously described (Grakoui et al., 1999). The purified I-E^k and ICAM-1 incorporated in dioleoylphosphatidylcholine liposomes (Avanti Polar Lipids, Inc.) were applied to cover glasses (thickness of 0.12–0.17 mm; Matsunami) or glass beads (4.86-µm sphere glass) to make the lipid bilayer containing 200 molecules of I-E^k and ICAM-1/μm^2 and incubated with Ag peptides (Yokosuka et al., 2005).

In this system, when 10 µM MCC(88-103) peptide was incubated at 37°C for 12 h, 8.9 ± 5.1% of total I-E^k was detected as peptide binding I-E^k (I-E^k + MCC; mean from three experiments) by staining with anti–I-E^k + MCC mAb D4 (Grakoui et al., 1999). Therefore, the concentration of I-E^k + MCC was 17.8/μm^2 for 10 µM. When we considered the general formula for affinity evaluation (K_d = [I-E^k]$_{free}$ × [MCC]$_{free}$/[I-E^k + MCC]) and the published K_d value of 0.54 µM, which was measured by using soluble I-E^k and MCC (Reay et al., 1992), the I-E^k + MCC concentrations for 1 µM, 100 nM, and 10 nM MCC were estimated to be 11.3, 2.94, and 0.34 μm^2, respectively.

Hepes-buffered saline containing 1% BSA, 1 mM $MgCl_2$, and 1 mM $CaCl_2$ was used for the assay. For immunohistochemistry, cells were placed on a planar bilayer for the indicated periods and then fixed with 2% paraformaldehyde at 37°C for 10 min. For FACS analysis, cells were spun down with the glass beads and incubated for 10–15 min and fixed with 2% paraformaldehyde at 37°C for 10 min. The cells were permeabilized in 0.05% digitonin or 0.1% Triton X-100 and stained with Abs in PBS containing 5% BSA. For calcium measurement, cells were incubated with 5 µM Fluo-4 AM and 10 µM Fura-red AM in 0.5% BSA containing PBS for 20 min at room temperature.

Fluorescence microscopy. A TIRF system (Olympus) was configured on a microscope (IX81). TIRF objective lenses (UAPON 100×, NA 1.49, oil; Olympus), dual excitation lasers, diode-pumped solid-state 488-nm and 561-nm laser systems (85BCD020 and 85YCA020; Melles Griot), and a charge-coupled device camera (ORCA flash4.0; Hamamatsu Photonics) were used. Dual-color videos were taken every 5 s for 10 min using Metamorph software (Molecular Devices). The images of the interaction between T cells and activated B cells that had been stimulated with LPS for 24 h were taken every 10 s using the IX81 microscope with an oil objective lens (Plan APO N 60×, NA 1.45; Olympus) under illumination with a Hg lamp. The intracellular calcium concentrations were also measured by using the IX81 microscope with Hg lamp illumination and an oil objective lens (UPlanAPO 40×, NA 1.00; Olympus). A microscope (TCS SP5; Leica Biosystems) with an oil immersion objective (HCX PL APO 100×, NA 1.44; Leica Biosystems) was used for fixed and stained samples. For detecting micro–adhesion rings formed in the cell–cell interaction, a hybrid detector (HyD; Leica Biosystems) was used to improve image quality.

Image analysis. IMARIS software (BitPlane) was used for counting and evaluation of fluorescent clusters. In this study, all the images were normalized using Fiji as follows: subtracted numerically until the mean background count became 10 and multiplied to adjust the count in the noncluster area of the cell to be 100. The criteria for a cluster was that the diameter was <5 µm, intensities at the center were >105–120 counts, and the summation of the fluorescence was >1,600–2,400 counts. The parameters were adjusted depending on the molecules being analyzed. The movements of the clusters were tracked automatically with an algorithm of Brownian movement, and the maximum gap distance in one frame was set as 5 µm.

Online supplemental material. Video 1 shows TCR-MCs transiently bordered by Pyk2 in the initial phase of activation. Video 2 shows different behaviors of ZAP70 and SLP76 clusters upon weak stimulation. Video 3 shows F-actin transiently accumulated at TCR-MCs in the initial phase of activation. Video 4 shows disappearance of SLP76 clusters and remaining TCR-MCs and ZAP70 clusters by CytD treatment. Video 5 shows the unstable contacts and impaired IS formation of dKD cells on the planer bilayer. Video 6 shows the unstable contacts and impaired IS formation of dKD cells upon interaction with APCs. Online supplemental material is available at http://www.jem.org/cgi/content/full/jem.20151088/DC1.

ACKNOWLEDGMENTS

We thank K. Shiroguchi for helpful discussion, M. Unno, W. Kobayashi, and N. Suzuki for technical support, and M. Yoshioka and H. Yamaguchi for secretarial assistance.

This work was supported by the Japan Society for the Promotion of Science KAK ENHI with Grants-in-Aid for Scientific Research to T. Saito ([S] JP24229004) and A. Hashimoto-Tane ([C] JP10415226) and partly by the Takeda Science Foundation (F1206042), Novartis Foundation, and Hayashi Memorial Foundation for Female Natural Scientists.

The authors declare no competing financial interests.

Author contributions: A. Hashimoto-Tane and T. Saito designed the studies. A. Hashimoto-Tane, M. Sakuma, and H. Ike performed experiments. T. Yokosuka provided advice and reagents. Y. Kimura and O. Ohara helped with molecular cloning. A. Hashimoto-Tane and T. Saito wrote the manuscript.

Submitted: 2 July 2015
Accepted: 13 May 2016

REFERENCES

Albiges-Rizo, C., O. Destaing, B. Fourcade, E. Planus, and M.R. Block. 2009. Actin machinery and mechanosensitivity in invadopodia, podosomes and focal adhesions. *J. Cell Sci.* 122:3037–3049. http://dx.doi.org/10.1242/jcs.052704

Baker, R.G., C.J. Hsu, D. Lee, M.S. Jordan, J.S. Maltzman, D.A. Hammer, T. Baumgart, and G.A. Koretzky. 2009. The adapter protein SLP-76 mediates "outside-in" integrin signaling and function in T cells. *Mol. Cell. Biol.* 29:5578–5589. http://dx.doi.org/10.1128/MCB.00283-09

Barda-Saad, M., A. Braiman, R. Titerence, S.C. Bunnell, V.A. Barr, and L.E. Samelson. 2005. Dynamic molecular interactions linking the T cell antigen receptor to the actin cytoskeleton. *Nat. Immunol.* 6:80–89. http://dx.doi.org/10.1038/ni1143

Beinke, S., H. Phee, J.M. Clingan, J. Schlessinger, M. Matloubian, and A. Weiss. 2010. Proline-rich tyrosine kinase-2 is critical for CD8 T-cell short-lived effector fate. *Proc. Natl. Acad. Sci. USA.* 107:16234–16239. http://dx.doi.org/10.1073/pnas.1011556107

Bunnell, S.C., D.I. Hong, J.R. Kardon, T. Yamazaki, C.J. McGlade, V.A. Barr, and L.E. Samelson. 2002. T cell receptor ligation induces the formation of dynamically regulated signaling assemblies. *J. Cell Biol.* 158:1263–1275. http://dx.doi.org/10.1083/jcb.200203043

Campi, G., R. Varma, and M.L. Dustin. 2005. Actin and agonist MHC-peptide complex-dependent T cell receptor microclusters as scaffolds for signaling. *J. Exp. Med.* 202:1031–1036. http://dx.doi.org/10.1084/jem.20051182

Čemerski, S., J. Das, J. Locasale, P. Arnold, E. Giurisato, M.A. Markiewicz, D. Fremont, P.M. Allen, A.K. Chakraborty, and A.S. Shaw. 2007. The stimulatory potency of T cell antigens is influenced by the formation of the immunological synapse. *Immunity.* 26:345–355. http://dx.doi.org/10.1016/j.immuni.2007.01.013

Collin, O., S. Na, F. Chowdhury, M. Hong, M.E. Shin, F. Wang, and N. Wang. 2008. Self-organized podosomes are dynamic mechanosensors. *Curr. Biol.* 18:1288–1294. http://dx.doi.org/10.1016/j.cub.2008.07.046

Comrie, W.A., A. Babich, and J.K. Burkhardt. 2015. F-actin flow drives affinity maturation and spatial organization of LFA-1 at the immunological synapse. *J. Cell Biol.* 208:475–491. http://dx.doi.org/10.1083/jcb.201406121

Crites, T.J., K. Padhan, J. Muller, M. Krogsgaard, P.R. Gudla, S.J. Lockett, and R. Varma. 2014. TCR microclusters pre-exist and contain molecules necessary for TCR signal transduction. *J. Immunol.* 193:56–67. http://dx.doi.org/10.4049/jimmunol.1400315

Dustin, M.L., and J.A. Cooper. 2000. The immunological synapse and the actin cytoskeleton: molecular hardware for T cell signaling. *Nat. Immunol.* 1:23–29. http://dx.doi.org/10.1038/76877

Dustin, M.L., S.K. Bromley, Z. Kan, D.A. Peterson, and E.R. Unanue. 1997. Antigen receptor engagement delivers a stop signal to migrating T lymphocytes. *Proc. Natl. Acad. Sci. USA.* 94:3909–3913. http://dx.doi.org/10.1073/pnas.94.8.3909

Eskan, M.A., R. Jotwani, T. Abe, J. Chmelar, J.H. Lim, S. Liang, P.A. Ciero, J.L. Krauss, F. Li, M. Rauner, et al. 2012. The leukocyte integrin antagonist Del-1 inhibits IL-17-mediated inflammatory bone loss. *Nat. Immunol.* 13:465–473. http://dx.doi.org/10.1038/ni.2260

Grakoui, A., S.K. Bromley, C. Sumen, M.M. Davis, A.S. Shaw, P.M. Allen, and M.L. Dustin. 1999. The immunological synapse: a molecular machine controlling T cell activation. *Science.* 285:221–227. http://dx.doi.org/10.1126/science.285.5425.221

Hashimoto-Tane, A., T. Yokosuka, K. Sakata-Sogawa, M. Sakuma, C. Ishihara, M. Tokunaga, and T. Saito. 2011. Dynein-driven transport of T cell receptor microclusters regulates immune synapse formation and T cell activation. *Immunity.* 34:919–931. http://dx.doi.org/10.1016/j.immuni.2011.05.012

Herreros, L., J.L. Rodríguez-Fernandez, M.C. Brown, J.L. Alonso-Lebrero, C. Cabañas, F. Sánchez-Madrid, N. Longo, C.E. Turner, and P. Sánchez-Mateos. 2000. Paxillin localizes to the lymphocyte microtubule organizing center and associates with the microtubule cytoskeleton. *J. Biol. Chem.* 275:26436–26440. http://dx.doi.org/10.1074/jbc.M003970200

Ilani, T., G. Vasiliver-Shamis, S. Vardhana, A. Bretscher, and M.L. Dustin. 2009. T cell antigen receptor signaling and immunological synapse stability require myosin IIA. *Nat. Immunol.* 10:531–539. http://dx.doi.org/10.1038/ni.1723

Jacobelli, J., S.A. Chmura, D.B. Buxton, M.M. Davis, and M.F. Krummel. 2004. A single class II myosin modulates T cell motility and stopping, but not synapse formation. *Nat. Immunol.* 5:531–538. http://dx.doi.org/10.1038/ni1065

Kaizuka, Y., A.D. Douglass, R. Varma, M.L. Dustin, and R.D. Vale. 2007. Mechanisms for segregating T cell receptor and adhesion molecules during immunological synapse formation in Jurkat T cells. *Proc. Natl. Acad. Sci. USA.* 104:20296–20301. http://dx.doi.org/10.1073/pnas.0710258105

Krummel, M.F., M.D. Sjaastad, C. Wülfing, and M.M. Davis. 2000. Differential clustering of CD4 and CD3ζ during T cell recognition. *Science.* 289:1349–1352. http://dx.doi.org/10.1126/science.289.5483.1349

Kumari, S., D. Depoil, R. Martinelli, E. Judokusumo, G. Carmona, F.B. Gertler, L.C. Kam, C.V. Carman, J.K. Burkhardt, D.J. Irvine, and M.L. Dustin. 2015. Actin foci facilitate activation of the phospholipase C-γ in primary T lymphocytes via the WASP pathway. *eLife.* 4:. http://dx.doi.org/10.7554/eLife.04953

Liu, X., T.M. Kapoor, J.K. Chen, and M. Huse. 2013. Diacylglycerol promotes centrosome polarization in T cells via reciprocal localization of dynein and myosin II. *Proc. Natl. Acad. Sci. USA.* 110:11976–11981. http://dx.doi.org/10.1073/pnas.1306180110

Mitra, S.K., D.A. Hanson, and D.D. Schlaepfer. 2005. Focal adhesion kinase: in command and control of cell motility. *Nat. Rev. Mol. Cell Biol.* 6:56–68. http://dx.doi.org/10.1038/nrm1549

Monks, C.R., B.A. Freiberg, H. Kupfer, N. Sciaky, and A. Kupfer. 1998. Three-dimensional segregation of supramolecular activation clusters in T cells. *Nature.* 395:82–86. http://dx.doi.org/10.1038/25764

Murphy, D.A., and S.A. Courtneidge. 2011. The 'ins' and 'outs' of podosomes and invadopodia: characteristics, formation and function. *Nat. Rev. Mol. Cell Biol.* 12:413–426. http://dx.doi.org/10.1038/nrm3141

Pauker, M.H., B. Reicher, S. Fried, O. Perl, and M. Barda-Saad. 2011. Functional cooperation between the proteins Nck and ADAP is fundamental for actin reorganization. *Mol. Cell. Biol.* 31:2653–2666. http://dx.doi.org/10.1128/MCB.01358-10

Perez, O.D., D. Mitchell, G.C. Jager, S. South, C. Murriel, J. McBride, L.A. Herzenberg, S. Kinoshita, and G.P. Nolan. 2003. Leukocyte functional antigen 1 lowers T cell activation thresholds and signaling through

cytohesin-1 and Jun-activating binding protein 1. *Nat. Immunol.* 4:1083–1092. http://dx.doi.org/10.1038/ni984

Peterson, E.J., M.L. Woods, S.A. Dmowski, G. Derimanov, M.S. Jordan, J.N. Wu, P.S. Myung, Q.H. Liu, J.T. Pribila, B.D. Freedman, et al. 2001. Coupling of the TCR to integrin activation by Slap-130/Fyb. *Science.* 293:2263–2265. http://dx.doi.org/10.1126/science.1063486

Reay, P.A., D.A. Wettstein, and M.M. Davis. 1992. pH dependence and exchange of high and low responder peptides binding to a class II MHC molecule. *EMBO J.* 11:2829–2839.

Robertson, L.K., and H.L. Ostergaard. 2011. Paxillin associates with the microtubule cytoskeleton and the immunological synapse of CTL through its leucine-aspartic acid domains and contributes to microtubule organizing center reorientation. *J. Immunol.* 187:5824–5833. http://dx.doi.org/10.4049/jimmunol.1003690

Robertson, L.K., L.R. Mireau, and H.L. Ostergaard. 2005. A role for phosphatidylinositol 3-kinase in TCR-stimulated ERK activation leading to paxillin phosphorylation and CTL degranulation. *J. Immunol.* 175:8138–8145. http://dx.doi.org/10.4049/jimmunol.175.12.8138

Rodríguez-Fernández, J.L., M. Gómez, A. Luque, N. Hogg, F. Sánchez-Madrid, and C. Cabañas. 1999. The interaction of activated integrin lymphocyte function-associated antigen 1 with ligand intercellular adhesion molecule 1 induces activation and redistribution of focal adhesion kinase and proline-rich tyrosine kinase 2 in T lymphocytes. *Mol. Biol. Cell.* 10:1891–1907. http://dx.doi.org/10.1091/mbc.10.6.1891

Roncagalli, R., S. Hauri, F. Fiore, Y. Liang, Z. Chen, A. Sansoni, K. Kanduri, R. Joly, A. Malzac, H. Lähdesmäki, et al. 2014. Quantitative proteomics analysis of signalosome dynamics in primary T cells identifies the surface receptor CD6 as a Lat adaptor-independent TCR signaling hub. *Nat. Immunol.* 15:384–392. http://dx.doi.org/10.1038/ni.2843

Sage, P.T., L.M. Varghese, R. Martinelli, T.E. Sciuto, M. Kamei, A.M. Dvorak, T.A. Springer, A.H. Sharpe, and C.V. Carman. 2012. Antigen recognition is facilitated by invadosome-like protrusions formed by memory/effector T cells. *J. Immunol.* 188:3686–3699. http://dx.doi.org/10.4049/jimmunol.1102594

Saito, T., and T. Yokosuka. 2006. Immunological synapse and microclusters: the site for recognition and activation of T cells. *Curr. Opin. Immunol.* 18:305–313. http://dx.doi.org/10.1016/j.coi.2006.03.014

Sancho, D., M. Nieto, M. Llano, J.L. Rodríguez-Fernández, R. Tejedor, S. Avraham, C. Cabañas, M. López-Botet, and F. Sánchez-Madrid. 2000. The tyrosine kinase PYK-2/RAFTK regulates natural killer (NK) cell cytotoxic response, and is translocated and activated upon specific target cell recognition and killing. *J. Cell Biol.* 149:1249–1262. http://dx.doi.org/10.1083/jcb.149.6.1249

Sancho, D., M.C. Montoya, A. Monjas, M. Gordón-Alonso, T. Katagiri, D. Gil, R. Tejedor, B. Alarcón, and F. Sánchez-Madrid. 2002. TCR engagement induces proline-rich tyrosine kinase-2 (Pyk2) translocation to the T cell-APC interface independently of Pyk2 activity and in an immunoreceptor tyrosine-based activation motif-mediated fashion. *J. Immunol.* 169:292–300. http://dx.doi.org/10.4049/jimmunol.169.1.292

Schmits, R., T.M. Kündig, D.M. Baker, G. Shumaker, J.J. Simard, G. Duncan, A. Wakeham, A. Shahinian, A. van der Heiden, M.F. Bachmann, et al. 1996. LFA-1-deficient mice show normal CTL responses to virus but fail to reject immunogenic tumor. *J. Exp. Med.* 183:1415–1426. http://dx.doi.org/10.1084/jem.183.4.1415

Springer, T.A., and M.L. Dustin. 2012. Integrin inside-out signaling and the immunological synapse. *Curr. Opin. Cell Biol.* 24:107–115. http://dx.doi.org/10.1016/j.ceb.2011.10.004

Tsuchida, M., S.J. Knechtle, and M.M. Hamawy. 1999. CD28 ligation induces tyrosine phosphorylation of Pyk2 but not Fak in Jurkat T cells. *J. Biol. Chem.* 274:6735–6740. http://dx.doi.org/10.1074/jbc.274.10.6735

van den Dries, K., M.B. Meddens, S. de Keijzer, S. Shekhar, V. Subramaniam, C.G. Figdor, and A. Cambi. 2013. Interplay between myosin IIA-mediated contractility and actin network integrity orchestrates podosome composition and oscillations. *Nat. Commun.* 4:1412. http://dx.doi.org/10.1038/ncomms2402

van Seventer, G.A., M.M. Mullen, and J.M. van Seventer. 1998. Pyk2 is differentially regulated by β_1 integrin- and CD28-mediated co-stimulation in human $CD4^+$ T lymphocytes. *Eur. J. Immunol.* 28:3867–3877. http://dx.doi.org/10.1002/(SICI)1521-4141(199811)28:11<3867::AID-IMMU3867>3.0.CO;2-K

Varma, R., G. Campi, T. Yokosuka, T. Saito, and M.L. Dustin. 2006. T cell receptor-proximal signals are sustained in peripheral microclusters and terminated in the central supramolecular activation cluster. *Immunity.* 25:117–127. http://dx.doi.org/10.1016/j.immuni.2006.04.010

Wang, Y., K. Shibuya, Y. Yamashita, J. Shirakawa, K. Shibata, H. Kai, T. Yokosuka, T. Saito, S. Honda, S. Tahara-Hanaoka, and A. Shibuya. 2008. LFA-1 decreases the antigen dose for T cell activation in vivo. *Int. Immunol.* 20:1119–1127. http://dx.doi.org/10.1093/intimm/dxn070

Webb, D.J., K. Donais, L.A. Whitmore, S.M. Thomas, C.E. Turner, J.T. Parsons, and A.F. Horwitz. 2004. FAK-Src signalling through paxillin, ERK and MLCK regulates adhesion disassembly. *Nat. Cell Biol.* 6:154–161. http://dx.doi.org/10.1038/ncb1094

Yokosuka, T., K. Sakata-Sogawa, W. Kobayashi, M. Hiroshima, A. Hashimoto-Tane, M. Tokunaga, M.L. Dustin, and T. Saito. 2005. Newly generated T cell receptor microclusters initiate and sustain T cell activation by recruitment of Zap70 and SLP-76. *Nat. Immunol.* 6:1253–1262. http://dx.doi.org/10.1038/ni1272

Yu, C.H., H.J. Wu, Y. Kaizuka, R.D. Vale, and J.T. Groves. 2010. Altered actin centripetal retrograde flow in physically restricted immunological synapses. *PLoS One.* 5:e11878. http://dx.doi.org/10.1371/journal.pone.0011878